



# Analysis of Compositional Effects on Global Flow Regimes in CO<sub>2</sub> Near-Miscible Displacements in Heterogeneous Systems

G. Wang<sup>1</sup> · G. E. Pickup<sup>1</sup> · K. S. Sorbie<sup>1</sup> · E. J. Mackay<sup>1</sup>

Received: 16 July 2018 / Accepted: 30 May 2019 / Published online: 12 June 2019  
© The Author(s) 2019

## Abstract

This study investigates the interaction of compositional effects with the flow behaviour during near-miscible (and immiscible) CO<sub>2</sub>–oil displacements in heterogeneous systems. A series of numerical simulations modelling 1D slim-tube and 2D areal systems were simulated using a fully compositional simulator. A number of grid resolutions for a slim-tube model were simulated to choose the proper level of numerical dispersion to mimic the actual physical dispersion. The corresponding 2D cases are based on a small heterogeneous sector model of dimensions 50 m × 10 m, in order that the fine-scale displacement physics can be modelled accurately. We investigated various flow regimes ranging from viscous fingering to channelling displacements within heterogeneous random correlated fields. We found that the reduced recovery is the result of a combination of differences in sweep efficiency associated with the viscous fingering and possible differences in local mixing that affect composition path. At the same time, the unstable phase flow determined by the underlying heterogeneity slows the flow in the unswept area and leads to unequal displacement performance between preferential and non-preferential routes. Specifically, lighter components have moved preferentially in high gas saturation zones, and leaving the heavier components behind in slower flow zones. In the case of channelling flow, compositional effects were less important since the permeability channel dominated the displacement. Both the ultimate oil recovery and component recovery are significantly and about equally reduced, when the underlying heterogeneity is of dominant influence. To summarise, compositional effects can have a very significant impact on the prediction of near-miscible CO<sub>2</sub> EOR projects. Issues such as front stability, local displacement efficiency and formation of fingering/channelling during CO<sub>2</sub> near-miscible displacement can lead to behaviour that is significantly different from immiscible flooding in these systems. The process of mass transfer between CO<sub>2</sub> and oil can be hampered to a certain degree by unstable flow depending on the level of heterogeneity. This leads to a further reduction in component recovery, particularly of the heavier components. The complete dataset and results of this study are available online as a model case example for compositional flows in heterogeneous systems (Wang et al. in "The analysis of compositional effects on global flow regimes in CO<sub>2</sub> near-miscible displacements in heterogeneous systems" dataset for paper SPE-190273, 2018. <https://doi.org/10.17861/fc1c90bb-9d3f-4a6c-9170-7b7fe10ec7b9>).

**Keywords** CO<sub>2</sub> near-miscible displacement · Compositional effects · Flow regime · Fine-scale simulation

## 1 Review of Flow Behaviour in a CO<sub>2</sub>–Oil System

CO<sub>2</sub> flooding and gas flooding in general have been studied for several decades. For example, Holm and Josendal (1974) discussed and summarised the various mechanisms occurring in CO<sub>2</sub>–oil systems. They described how CO<sub>2</sub> enhances the oil recovery by solution gas drive, swelling of oil, reduction in viscosity and, most importantly, compositional effects, e.g. stripping of hydrocarbons. In their study, the procedures of slim-tube tests became established, and have generally been used to measure the minimum miscible pressure since then. They also investigated the effect of oil constituents on achieving miscibility between CO<sub>2</sub> and oil (Holm and Josendal 1982). They found that gasoline-range hydrocarbons are particularly efficient in achieving miscibility.

CO<sub>2</sub> flooding and gas flooding in general occur at an unfavourable mobility ratio, which may trigger fingering flow (Stalkup 1983). Gardner and Ypma (1984) performed 2D areal simulations to examine the effect of viscous instability in a first-contact miscible (FCM) displacement. They found that transverse mixing between CO<sub>2</sub> in a finger and oil in a neighbouring unswept zone could reduce the local displacement efficiency. This is because oil which has entered a finger due to transverse mixing, encounters fresh CO<sub>2</sub> rather than CO<sub>2</sub> enriched with light elements. Waggoner et al. (1992) analysed the competition between effects of adverse mobility ratio and heterogeneous permeability during FCM displacement. A set of simulations varying mobility ratio and level of heterogeneity was performed to reveal the different sources of fingering and channelling. The distinction between channelling and fingering is that fingering occurs due to viscous instability, while channelling is due to heterogeneity. They found that channelling occurs when the correlation range of the permeability field is of the order of the system length, even with unit mobility ratio. Chang et al. (1994) investigated phase-behaviour effects on finger formation. Their simulations of multiple-contact miscible CO<sub>2</sub> displacement showed that the component transfer between oil and CO<sub>2</sub> causes viscosity contrast and the capillary force to decrease simultaneously. Both effects tended to reduce the growth of fingering in their 2D results. However, due to the limitations of the computational power at that time, the grid resolution ( $\Delta x = 12.5$  ft.) of their simulations was probably insufficient to fully capture the details of compositional effects.

Stalkup (1990) investigated the effects of gas enrichment in reservoir-scale displacements using a compositional simulator with the Peng–Robinson equation of state. His results have shown that the predicted incremental oil recovery due to the gas enrichment is very sensitive to the numerical dispersion, which acts in a similar manner to the physical dispersion. Sorbie and Mackay (2000) investigated the possible scaling issues (not discussed here though) due to the in situ mixing between connate water and the injected water. They claimed that it is important to incorporate the correct level of dispersivity to model a displacement process correctly. Jessen et al. (2004) investigated the effect of the coarse grid on the composition path along a slim tube and the oil recovery in 2D models. Since they did not differentiate the source of discrepancies between the reduced heterogeneity and increased numerical dispersion in their upscaled cases, we believed that it is justified to take a further look at the interplay between compositional effects and global flow regimes (such as fingering and channelling), assuming a certain level of dispersion. As motivated

by their studies, we reproduced the dispersion effects through introducing the appropriate level of numerical simulations; however, we fully validate this with numerical tests using actual dispersion. Detailed discussions are presented in subsequent sections of the paper.

In a recent paper, Moortgat (2016) described a series of sensitivity tests on viscous and gravitational fingering accounting for mechanical dispersion, Fickian diffusion, flow rate and heterogeneity. His study focused on the effect of changed viscosity and density on the formation of fingering. He concluded that the fingering flow at near-miscible conditions could be profoundly different from FCM conditions and immiscible conditions presented in earlier studies. However, the details of the compositional effects such as the modified composition path were not included in his study. The effect of component transfer in a multi-dimensional system (such as a real reservoir) is still an issue.

The above review is presented to put the current study into the context of earlier work, which is relevant to the compositional effects occurring in CO<sub>2</sub> displacement. Our survey of the literature indicates that the interactions between global flow regimes and the compositional effects have not been fully investigated, particularly when compositional effects and heterogeneities are both important, such as in near-miscible CO<sub>2</sub> displacement. Therefore, we considered the following questions in this study:

- How do compositional effects interact with the underlying heterogeneity pattern of the flow field, particularly in the flow regimes of fingering and channelling?
- What are the overall influences on the local displacement efficiency and the ultimate oil/component recovery?
- How can we consistently measure and evaluate the compositional effects, and thus assess the accuracy of simulations using models at different scales and dimensions?

## 2 Methodology

### 2.1 1D Slim-Tube

A very fine-scale slim-tube model (i.e.  $\Delta x = 0.001$  m) was used to demonstrate the process of mass transfer (CO<sub>2</sub> displacing oil). Note that refining the cell size further has negligible influence on the results and therefore we assume it is a dispersion-free process. A tracer analysis (H<sub>2</sub>O\* displacing H<sub>2</sub>O) was also performed to determine the proper cell size to introduce a certain level of numerical dispersion, which was used to mimic the realistic physical dispersion in the subsequent 2D analysis. The whole length of the slim-tube simulation model here (50 m) was longer than a conventional slim tube to reduce the possible fluctuations in the numerical results (Fig. 1). More importantly, the results achieved in 1D tests can be directly compared to the subsequent 2D tests with the same “well spacing”.

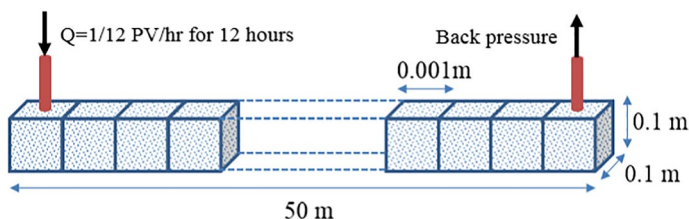
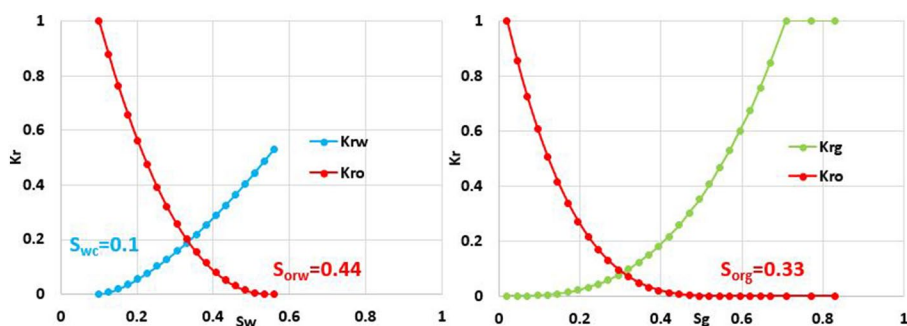


Fig. 1 Schematic of slim-tube model

**Table 1** Equation-of-state parameters for different components used in the simulation study

Parameter, unit	Component						
	CO <sub>2</sub>	N <sub>2</sub> to CH <sub>4</sub>	C <sub>2</sub> to C <sub>4</sub>	C <sub>5</sub> to C <sub>7</sub>	C <sub>8</sub> to C <sub>12</sub>	C <sub>13</sub> to C <sub>19</sub>	C <sub>20</sub> to C <sub>30</sub>
Mole fraction, %	1.2	11.7	19.5	22	28.2	9.4	8.1
Critical <i>P</i> , atm	72.8	45.2	41.9	31.3	23.9	17.2	11.9
Critical <i>V</i> , m <sup>3</sup> /k-mol	0.094	0.099	0.206	0.333	0.458	0.766	1.260
Critical <i>T</i> , deg K	304.2	189.7	338.4	556.9	667.5	769.0	801.5
Acentric factor	0.225	0.008	0.148	0.249	0.328	0.567	0.942
Mw, gm/gmol	44.0	16.2	44.8	83.5	120.5	210.7	401.9
Volume shift	−0.082	−0.154	−0.085	−0.009	0.044	0.130	0.269
Parachor	78.0	76.5	150.5	248.5	344.9	570.1	905.7
Omega A	0.457	0.457	0.549	0.457	0.457	0.457	0.457
Omega B	0.078	0.078	0.093	0.078	0.078	0.078	0.078
δ <sub>CO<sub>2</sub>-i</sub>	0.000	0.104	0.124	0.129	0.150	0.080	0.130

**Fig. 2** Oil–water and gas–oil relative permeability curves

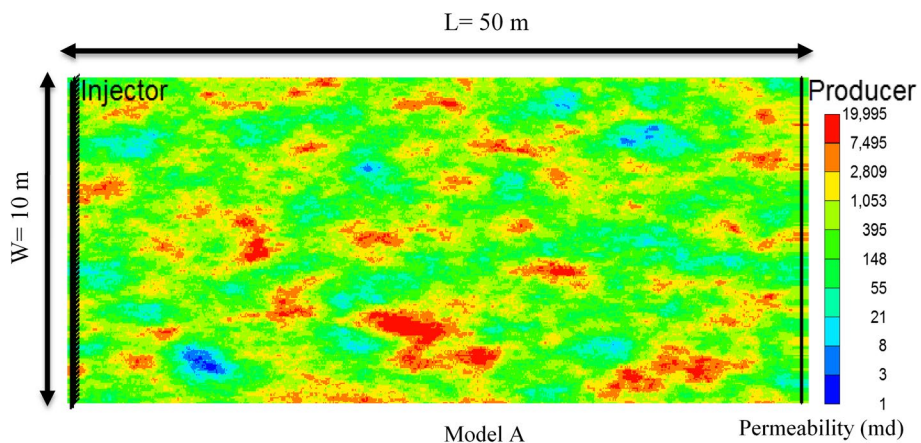
The porosity and permeability were homogeneous and set to 0.1 and 1 Darcy, respectively (Yellig and Metcalfe 1980; Khabibullin et al. 2017).

Table 1 shows the data for a seven-component light oil with a minimum miscibility pressure (MMP) of 125 bar. This 7-component lumped oil was based on a 34-component oil (see “Appendix 1”), which was provided to us by a sponsor company. In fact, we also tried the typical lumping strategy consisting of 4 pseudo-components, such as CO<sub>2</sub>, CH<sub>4</sub>, C<sub>2-7</sub> and C<sub>8+</sub> to reduce the compositional cost (Orr 2007). However, we found that the 4-component system in our case is not able to properly reflect an important phenomenon, namely that most of the oil can be stripped but heavy components (such as C<sub>20+</sub>) may be left behind in slim tube during near-miscible CO<sub>2</sub> displacement (See “Appendix 2”). Therefore, a 7-component system is used here, and the given data in Table 1 are applied to generate the PVT behaviour using the Peng–Robinson equation of state (EOS). The bubble point pressure was 38.5 bar at 53 °C. Oil viscosity was calculated using the Jossi, Stiel and Thodos’ correlation with an initial value of 0.16 mPa s (CMG 2017). The relative permeability curves used here are shown in Fig. 2. Note that a relatively high Sor (to immiscible gas) is chosen here (Sor=0.33) to give a higher target oil for stripping by compositional

effects, and this emphasises the magnitude of compositional effects on oil recovery. At this stage, neither hysteresis/capillary effects nor low-interfacial effects on the relative permeabilities are included in this study. We used adaptive implicit modes which can optimise both the computational cost and simulation stability. This method entails switching from IMPES to a fully implicit formulation in the cells where the global mole fraction exceeds 0.15 (CMG 2017). The maximum time step is set to  $5e-6$  day leading to a Courant number of 0.5. We also specified the maximum changes in global mole fraction during Newtonian iterations. If the change of global mole fraction of any component exceeds 0.5, the timestep size is reduced and the timestep is repeated. Note that refining the time step further or reducing the maximum change of global mole fraction made an insignificant change in the results and hence our simulations are essentially fully converged with this numerical control.

### 3 2D Areal Models

Lastly, we simulated near-miscible  $\text{CO}_2$  displacements for unfavourable mobility ratios in 2D areal random correlated systems. Two heterogeneous permeability fields were generated based on Dykstra–Parsons ( $V_{DP}$ ) coefficients (Dykstra and Parsons 1950) and dimensionless correlation ranges ( $R_L$ ). Model A which had a relatively short correlation length (0.1 of the system length) was generated to trigger possible fingering flow (Fig. 3), while Model B had a longer correlation length (of order the system length), thus leading to channelling flow (Fig. 4). All the other simulation settings, such as the EOS, were taken from the previous slim-tube tests. The injector in our tests was set to inject pure  $\text{CO}_2$  at a rate of 0.4 PV/d at reservoir conditions for 2.5 days (1PV in total) and the producer was controlled by setting the minimum bottom-hole pressure. Both wells were horizontal and were perforated along the width of the model. A set of parameters such as the residual oil saturation in representative cells and oil/component recovery were compared between the 1D and 2D tests.



**Fig. 3** Permeability field A ( $V_{DP}=0.7$ ,  $R_L=0.1$ ) used to trigger the fingering flow

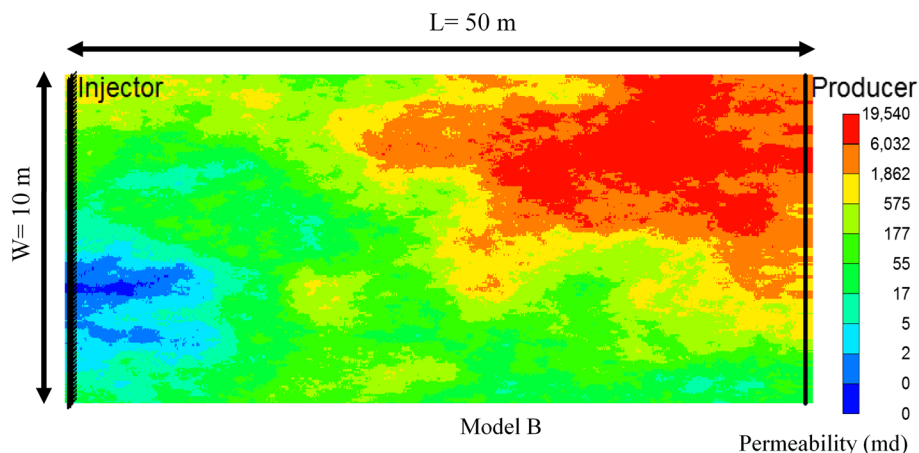


**Fig. 4** Permeability field B ( $V_{DP}=0.7$ ,  $R_L=1$ ) used to trigger the channelling flow

## 4 Results and Discussion

### 4.1 Component and Phase Distribution Along Slim Tube

In order to understand the details of component transfer, we compared the component and phase distribution along a slim tube between immiscible (70 bar) and near-miscible (120 bar) conditions. Two snapshots of the phase and component distributions are taken at 0.6 PVI before  $\text{CO}_2$  breakthrough and stacked together as seen in Fig. 5.

At immiscible conditions, limited amounts of light and medium oil components are vaporised into  $\text{CO}_2$ . A frontal dry gas bank (mainly methane) was found; this phenomenon has been well analysed in previous studies (Stalkup 1983; Orr 2007). The dry gas bank flows at a much lower viscosity and overtakes the oil at the front, which may have an adverse effect on the sweep efficiency in reality. Compared with immiscible displacement, more vaporised oil components are present in the gas phase at near-miscible conditions. There is very little oil left behind the displacing front. The remaining oil mainly consists of heavy components (C20–C30 here) and the dissolved  $\text{CO}_2$ . In other words, the rest of the oil components have been stripped and recovered. In addition, the resulting gas saturation is much higher at near-miscible conditions due to the vaporised oil components. This effect might further aggravate the instability in multi-phase flow in realistic (multi-dimensional) simulations since the gas is much more mobile than the oil. Note Fig. 5 is presented here to qualitatively show the different level of mass transfer process between immiscible and near-miscible displacements rather than for detailed calculations. For this reason, the details such as the smearing-out of the displacing front are not included.

### 4.2 Composition Path

In the previous section, we analysed the component distribution in all of the cells along the slim tube at one particular time. Here, we consider the component constitutions of a certain cell through the whole injection process. The aim of this part is to track the compositional

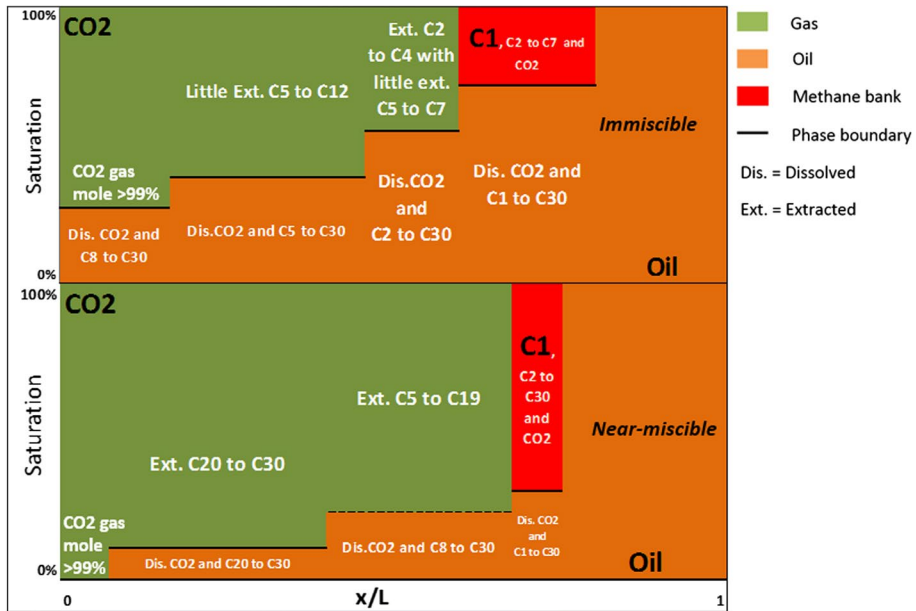


**Fig. 5** Component distribution along slim-tube after 0.6 PVI at immiscible (top) and near-miscible (bottom) conditions

variations of phases using ternary diagrams to evaluate the compositional effects. The dynamic fluid behaviour of  $\text{CO}_2$  displacement with three pseudo components ( $\text{CO}_2$ , C1–7 and C8+) is presented. The compositional paths for both oil and gas were investigated for a representative cell (15 m from the injector), at both immiscible and near-miscible conditions. The representative cell selected here was designed to experience the full composition path during 1PV injection, but not to be dominated by  $\text{CO}_2$  instantly.

As shown in Fig. 6, the oil and gas composition can be very similar at the early stage of the contact through the process of mass transfer under near-miscible conditions. The oil composition will be getting heavier again with the process of mass transfer. This is because most of the oil components have been recovered leaving C20+ behind. On the other hand, the stripping effect of the oil components has very limited impact at immiscible conditions. It also explains why most of the medium-to-heavy components are left behind at immiscible conditions along the slim tube. At the same time, the amount of  $\text{CO}_2$  dissolution is also limited through the whole injection process at immiscible conditions. At near-miscible conditions, a greater amount  $\text{CO}_2$  dissolution occurs and  $\text{CO}_2$  displacement is able to vaporise C1–7 from the oil phase almost completely after 1 PVI. As expected, much higher local displacement efficiency (remaining oil saturation close to 0 in this cell) can be achieved at near-miscible conditions than at immiscible conditions (as seen in Fig. 7).

### 4.3 Dispersion in the Model

In the previous section, we investigated the process of mass transfer (reflected by the composition path in a ternary diagram) using a very fine-scale (essentially dispersion-free) slim-tube model. However, in reality, we expect some level of physical (dispersion-like)



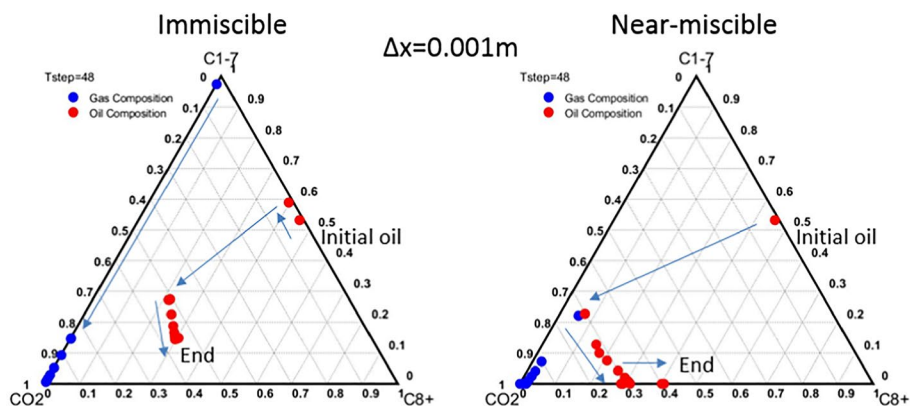
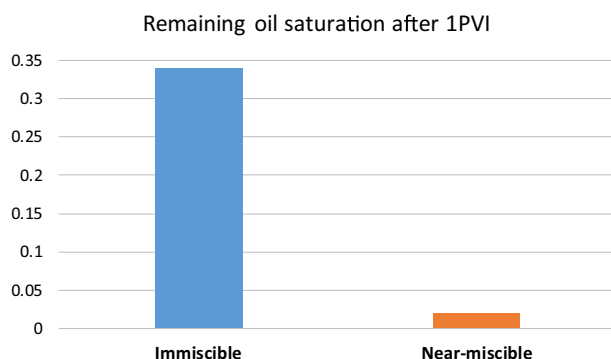


**Fig. 6** Oil and gas composition path of the representative cell in the slim tube at immiscible (left) and near-miscible conditions (right)

**Fig. 7** Remaining oil saturation of the representative cell at immiscible (left) and near-miscible conditions (right) in the slim-tube model



local mixing in the system (Stalkup 1998). According to Arya et al. (1988) and Sorbie and Mackay (2000), the actual level of mixing in reservoirs should be 0.01–2 m at the scale of 10–100 m (50 m here). Here, we assumed a dispersivity ( $\alpha_L$ ) of 0.025 m (CMG 2017) and performed a tracer simulation ( $H_2O^*$  displacing  $H_2O$ ) for various cell sizes, with the aim of using numerical dispersions to mimic the physical dispersions.

As seen in Fig. 8, the results from our finest model ( $\Delta x = 0.001$  m) with assumed dispersivity (0.025 m) correctly converges with the coarser model ( $\Delta x = 0.05$  m) with no added dispersivity; recall that the dispersivity should be  $\alpha = \Delta x/2$ . Hence, the slightly coarser grid ( $\Delta x = 0.05$  m) will be used to mimic “realistic” (i.e. “reservoir-like”) dispersivities for the subsequent 2D analysis. According to Jessen et al. (2004), the compositional effects can be very sensitive to dispersions, which will disrupt the shock structure and lead to lower levels of local stripping.

We believe that the first steps in upscaling near-miscible oil displacements by  $CO_2$  from the slim tube to a medium-sized grid block scale can be represented by these calculations. That is, some of the effects we model which show the mixing and interaction between fluid flow and the changes in compositional paths should at least qualitatively, be as they occur in reality. One of motivations of this study is to provide *input* for any potential upscaling methods considering mass transfers. Here, we also present comparison of displacement



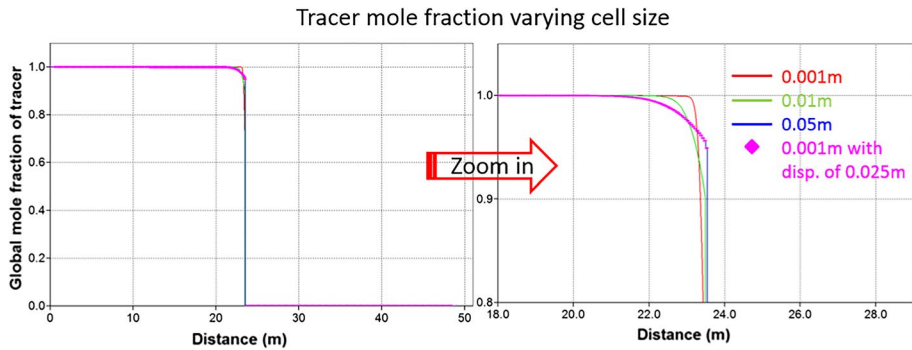


**Fig. 8** Snapshots of tracer mole fraction along the slim-tube varying cell size taken at 0.4 PVI

performance between models with the cell sizes of 0.001 m and 0.05 m, respectively (Fig. 9).

As seen in Fig. 9, the near-miscible displacement is more sensitive (as expected) than the immiscible displacement (discrepancy less than 1% between two immiscible curves). The oil recovery factor after 1 PVI decreases from 96 to 89% under near-miscible conditions. Clearly, the displacement performance has been degraded due to the artificial dispersion. Such effects have been well analysed by Orr (2007), although they are highly case dependent on the oil composition. Here, we present the composition path of the model with the cell size of 0.05 m, which serves as a reference for the subsequent 2D heterogeneous models. As seen in Figs. 6 (left) and 10 (left), the composition path of immiscible displacement is almost identical for cell sizes of 0.001 m and 0.05 m. On the other hand, there is an observable discrepancy between the gas and oil composition of the coarser-grid model ( $\Delta x = 0.05$  m) and the finer model ( $\Delta x = 0.001$  m), particularly at the early contact of the displacement under near-miscible conditions, as seen in Figs. 6 (right) and 10 (right).

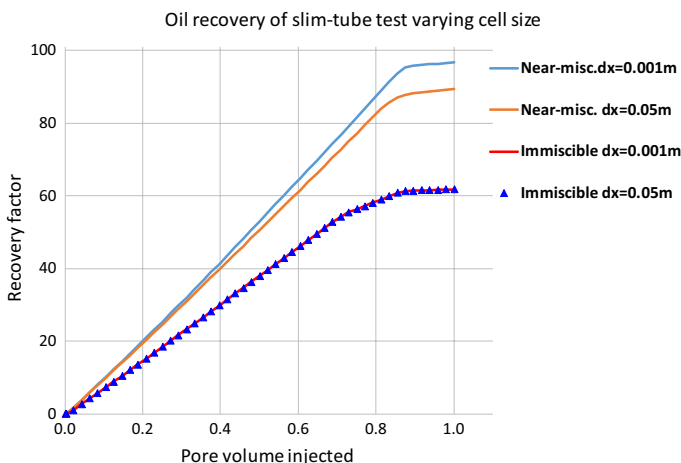


**Fig. 9** Oil recovery of slim-tube tests with PVI varying cell size in the flow direction ( $\Delta x$ )

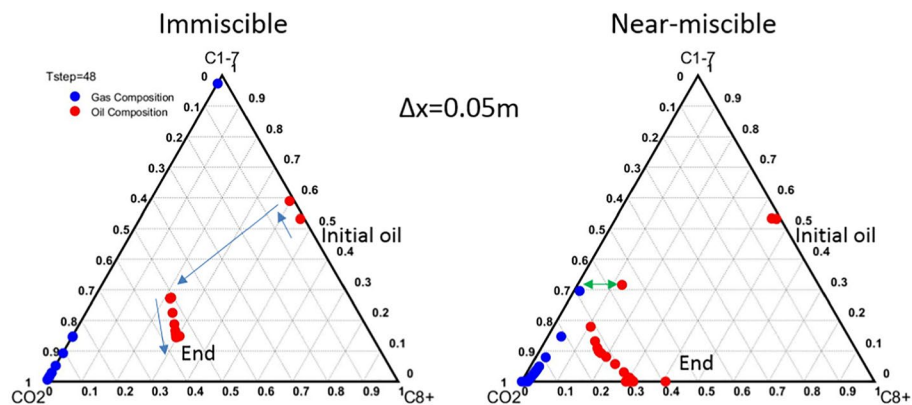


**Fig. 10** Oil and gas composition paths of the representative cell in the slim tube at immiscible (left) and near-miscible conditions (right) with the cell size of 0.05 m

#### 4.4 Fingering Flow Regime

Keeping the previous points in mind, we now present results for flow simulations in our 2D “reservoir” system (50 m × 10 m) using heterogeneous correlated random permeability fields with short and long correlation lengths. The shorter-correlation-length (5 m here) system leads to fingering flow whereas the longer correlation length (50 m here) induces channelling flow, as described below. The results from model A (Fig. 3) are presented first. Due to the unfavourable mobility ratios between gas and oil, typical fingering flow behaviour occurs for both immiscible and near-miscible flow. Note that a separate test with the unit mobility ratio on this permeability field presents a fairly stable front without any finger formation.

As shown in Fig. 11, it is not surprising that the oil recoveries in our 2D tests are worse than the slim-tube test. As seen in Fig. 12, multiple gas fingers (as expected) have been developed under both immiscible and near-miscible conditions. However, the difference in the reduction of the oil recovery under immiscible/near-miscible conditions compared with the slim-tube tests deserves a further analysis. The lowered oil recovery under near-miscible conditions is more than double that under immiscible displacement. We conjectured that the reduced recovery is the result of a combination of differences in sweep efficiency associated with the viscous fingering and possible differences in local mixing that affect the composition path. In order to test our conjecture, two typical areas (i.e. in a non-preferential and a preferential route) were investigated using a similar workflow as the slim-tube tests. We present the composition path of 3 cells in a row (0.5 m between each cell) in each streamline indicated by the black oval shapes.

As seen in Fig. 13 (left), the compositional path of the selected preferential route is very similar to the slim-tube test with negligible discrepancy. On the other hand (Fig. 13 right), the later stages of both the oil and the gas composition path are largely missing in the non-preferential route, which indicates that the journey along the composition path is not complete. In other words, the unstable phase flow determined by the underlying heterogeneity slows the flow in the unswept area and leads to unequal displacement performance between preferential and non-preferential routes. In fact, we believe this is a typical example of how the phase flow interacts with compositional effects.

The component recoveries for the slim-tube and 2D tests are shown in Fig. 14. In the case of immiscible displacement, the reduction in recovery does not vary much with

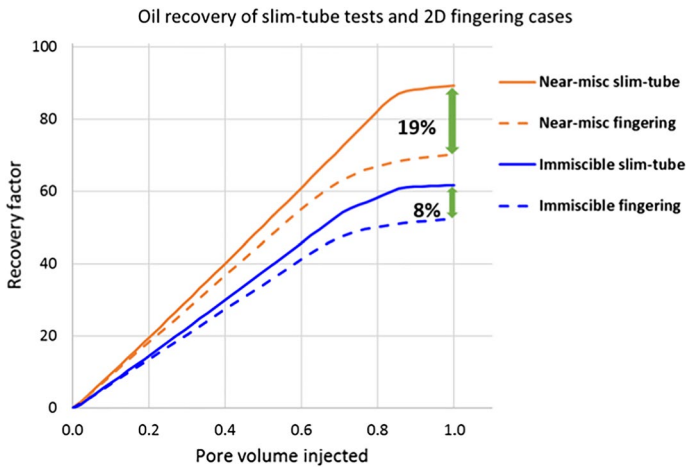


**Fig. 11** Oil recovery from slim-tube tests (ST) and fingering cases after 1 PVI under immiscible and near-miscible conditions

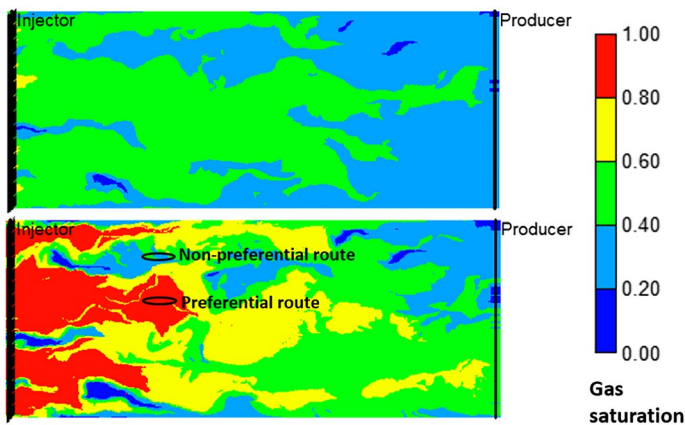


**Fig. 12** Snapshot of gas saturation after 1 PVI under immiscible (top) and near-miscible conditions (bottom)

components. On the other hand, there is a greater reduction in the recovery of the heavier components. This is because near-miscible  $\text{CO}_2$  displacement relies on a continuous process of mass transfer between gas and oil. Lighter components have moved preferentially in high gas saturation zones, and the heavier components left behind in slower flow zones have not been produced.

#### 4.5 Channelling Flow Regime

Due to the dominant heterogeneity in the system with a longer correlation length, typical channelling flow occurs both in immiscible and near-miscible cases, as seen in Fig. 15. The flow in such a system (dominant channel flow) is quite similar to the flow in a stratified formation, and it leads to early  $\text{CO}_2$  breakthrough and very poor sweep efficiency. As a

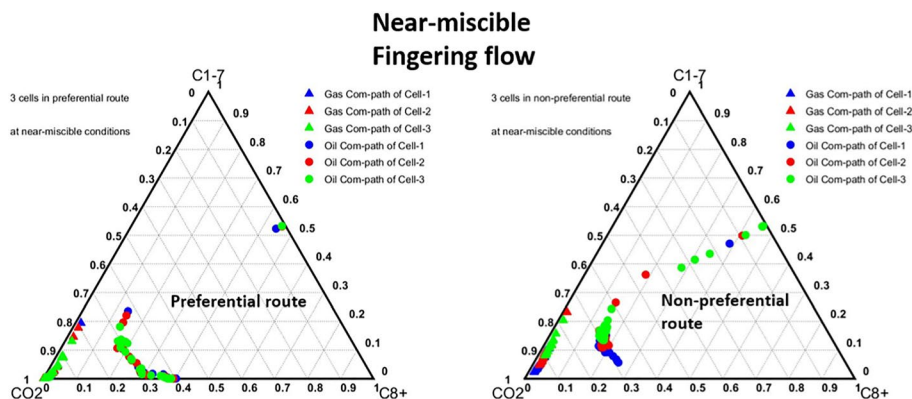


**Fig. 13** Comparisons of composition path between preferential (left) and non-preferential route (right) in the 2D areal heterogeneous system

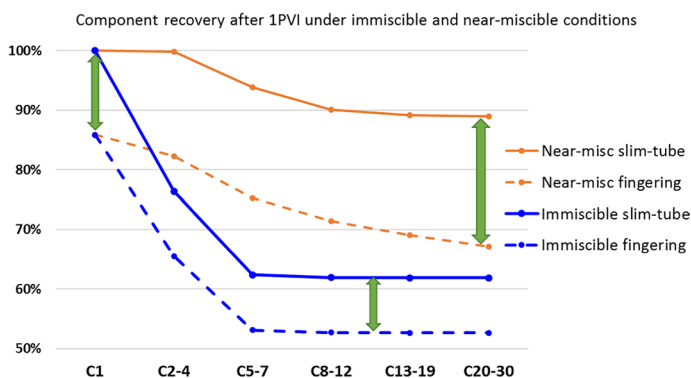


**Fig. 14** Comparisons of component recoveries between slim-tube (ST) tests and fingering cases under immiscible (blue) and near-miscible conditions (orange)

result, the oil recoveries after 1 PVI in our channelling cases are much lower than in the 1D tests under both conditions. Interestingly, the overall sweep of near-miscible displacement is rather worse than the immiscible displacement. This because the significant oil vaporisation during near-miscible displacement increases the gas saturation and therefore leads to more severe channelling flow, which greatly suppresses the crossflow. Therefore, the net result of the decreased sweep but improved local displacement efficiency leads to a very limited recovery improvement, as seen Fig. 16.

Similar to the previous analysis of the fingering flow, we present the composition path of 3 cells in a row (0.5 m between each cell) in two streamlines, indicated by black oval shapes, i.e. non-preferential and the flow boundary of the channel, respectively. As expected, the composition path of the preferential route (Fig. 17 left) is most similar to the slim-tube test whereas the one at the flow boundary (Fig. 17 right) is much less complete. Unlike the fingering case, the medium-heavy component recovery is not reduced more than the lighter components (Fig. 18). In other words, compositional effects are less affected in the swept zone, where evident channelling flow occurs. Both the ultimate oil recovery and

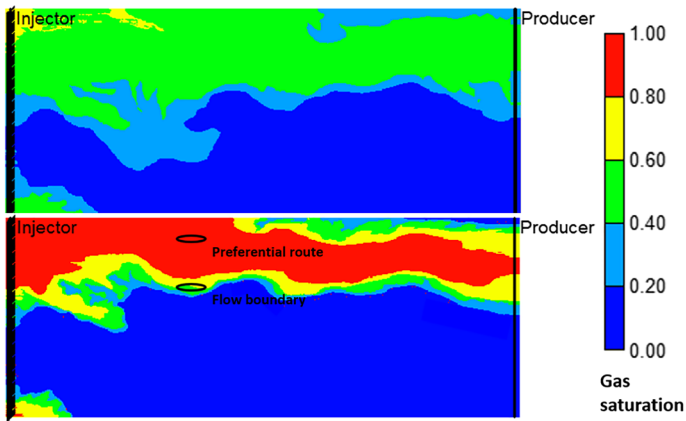


**Fig. 15** Snapshot gas saturation after 1 PVI under immiscible conditions (top) and near-miscible (bottom) conditions

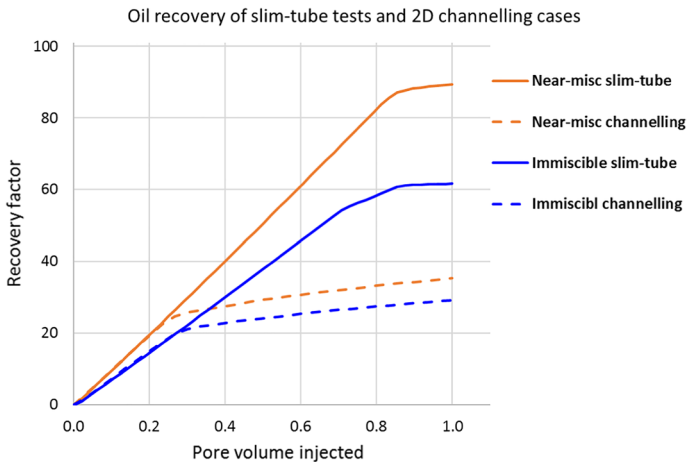


**Fig. 16** Oil recovery of slim-tube tests and channelling cases after 1 PVI under immiscible and near-miscible conditions

component recovery are significantly and about equally reduced, when the underlying heterogeneity is of dominant influence.

## 5 Summary and Conclusions

The central intention of this paper is to study how compositional effects contribute to oil displacement by  $\text{CO}_2$ , firstly in a 1D slim-tube model and then in 2D areal heterogeneous models. In the absence of mixing (dispersion), certain shocks are known to occur in 1D multi-component near-miscible displacements of this type as extensively described by Orr (2007). However, in real systems there is always some level of mixing by various mechanisms, e.g. dispersivity, heterogeneity and viscous fingering. This mixing will disrupt the shock structure, alter phase paths in a slim-tube model and consequently can reduce oil

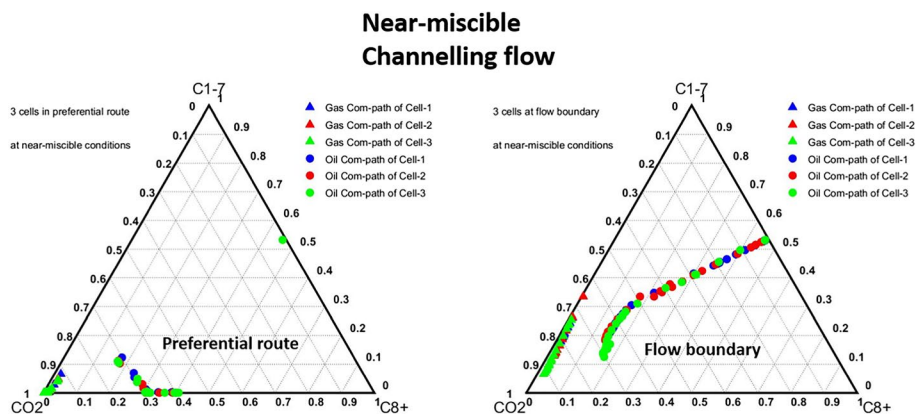


**Fig. 17** Comparisons of composition path between preferential (left) and flow boundary of the channel (right) in the 2D areal heterogeneous system

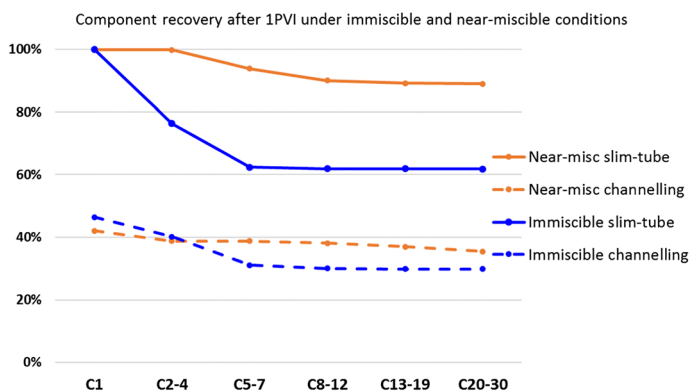


**Fig. 18** Comparisons of component recoveries between slim-tube tests and channelling cases

recovery by suppressing component stripping. In the models used in this work, we used very fine grids but with some level of mixing at a “realistic” reservoir scale ( $\alpha_L = 0.025$  m). This can be done by using a very small (50 m  $\times$  10 m) “reservoir” model. Indeed, the model is more like a medium-sized single grid block and this allows us to use realistic levels of mixing (dispersivities). Using these models, we can compare the phase and component compositional paths observed for a typical grid block in a slim-tube calculation, with those in 2D heterogeneous systems with different permeability structures that exhibit both fingering and channelling flow regimes. The cases of “composition only” in this study provide a baseline for any other mechanism to be imposed, such as interfacial tension effects, gravity and hysteresis (if WAG is applied). Very importantly, the analysis of the dynamic compositional path and component recovery, also leads us to a new workflow and criteria to measure the potential discrepancies between the laboratory-scale phenomena and reservoir behaviour (or simply between different scales). This is especially relevant when both compositional effects and heterogeneity are important, such as in near-miscible  $\text{CO}_2$  displacement. In forthcoming papers (Wang et al. 2019a, b), we will significantly extend this work to consider water–alternating gas (WAG) displacements including IFT (film flow) effects. Here, by comparing

simulations of oil displacement by CO<sub>2</sub> in these different 2D systems, we make 3 observations of how the compositional effects interact with the flow regimes.

1. The composition path in the 2D areal system does not follow the same composition path as in the slim-tube tests, particularly in the later stages. Various types of mixing such as dispersivity (substituted by numerical dispersions here), heterogeneity and viscous fingering can slow the process of component stripping and thus lower the displacement efficiency. In particular, heavier component recovery is more likely to be influenced in typical flow fingering regimes.
2. Compositional effects are of much less importance when channelling flow occurs. The strong oil vaporisation can further aggravate the flow channel in our case and therefore suppress crossflow. The net result of the decreased sweep but improved local displacement efficiency leads to a very limited recovery improvement.
3. Assuming a certain level of mixing, a 1D slim-tube test is able to represent a preferential flow route (well-swept area) in a multi-dimensional system regarding the local displacement efficiency for the same amount of injection. However, the overall displacement performance is highly dependent on the interaction of fingering/channelling flow, crossflow, and compositional effects.

**Acknowledgements** The authors would like to gratefully acknowledge the funding for this study by the sponsor of the “Best in Class Predictions of Enhanced Oil Recovery Using CO<sub>2</sub> Injection” project at Heriot-Watt University (Petronas and Uzma). Energi Simulation is thanked for funding the chair in Reactive Flow Simulation at Heriot-Watt University held by Eric Mackay. CMG is thanked for use of the GEM compositional simulator. Finally, we would also like to thank the reviewers for their useful comments.

**Open Access** This article is distributed under the terms of the Creative Commons Attribution 4.0 International License (<http://creativecommons.org/licenses/by/4.0/>), which permits unrestricted use, distribution, and reproduction in any medium, provided you give appropriate credit to the original author(s) and the source, provide a link to the Creative Commons license, and indicate if changes were made.

## Appendix 1

Fluid characterisation.

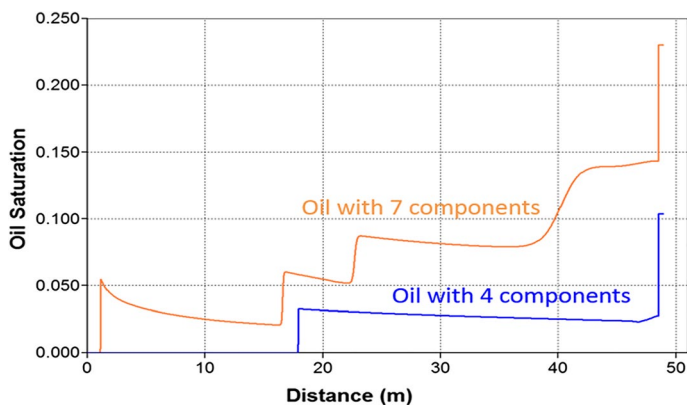
Component	Mass frac.	Mole frac.	MW	SG	Tb(C)
CO <sub>2</sub>	0.0045	0.0118	44.0095	0.8180	− 78.4643
N <sub>2</sub>	0.0004	0.0016	28.0135	0.8094	− 195.8100
C <sub>1</sub>	0.0160	0.1154	16.0425	0.3000	− 161.5167
C <sub>2</sub>	0.0156	0.0601	30.0690	0.3562	− 88.6056
C <sub>3</sub>	0.0247	0.0648	44.0956	0.5070	− 42.0833
<i>i</i> -C <sub>4</sub>	0.0112	0.0222	58.1222	0.5629	− 11.7889
<i>n</i> -C <sub>4</sub>	0.0239	0.0476	58.1222	0.5840	− 0.5111
<i>i</i> -C <sub>5</sub>	0.0205	0.0328	72.1488	0.6247	27.8444
<i>n</i> -C <sub>5</sub>	0.0231	0.0370	72.1488	0.6311	36.0667
C <sub>6</sub>	0.0464	0.0651	82.2600	0.6960	63.8889
C <sub>7</sub>	0.0670	0.0842	91.9314	0.7400	91.9444
C <sub>8</sub>	0.0883	0.0989	103.1156	0.7659	116.6667



Component	Mass frac.	Mole frac.	MW	SG	Tb(C)
C9	0.0770	0.0784	113.4302	0.8129	142.2222
C10	0.0589	0.0515	132.0084	0.7937	165.8333
C11	0.0399	0.0313	147.0000	0.7930	187.2222
C12	0.0297	0.0213	161.0000	0.8040	208.3333
C13	0.0293	0.0193	175.0000	0.8150	227.2222
C14	0.0238	0.0145	190.0000	0.8260	246.3889
C15	0.0239	0.0134	206.0000	0.8360	266.1111
C16	0.0205	0.0106	222.0000	0.8430	283.3333
C17	0.0185	0.0090	237.0000	0.8510	300.0000
C18	0.0210	0.0097	251.0000	0.8560	312.7778
C19	0.0186	0.0082	263.0000	0.8610	325.0000
C20	0.0127	0.0053	275.0000	0.8660	338.0556
C21	0.0100	0.0040	291.0000	0.8710	351.1111
C22	0.0084	0.0032	300.0000	0.8760	363.3333
C23	0.0064	0.0024	312.0000	0.8810	375.0000
C24	0.0056	0.0020	324.0000	0.8850	386.1111
C25	0.0054	0.0019	337.0000	0.8880	397.2222
C26	0.0056	0.0019	349.0000	0.8920	407.7778
C27	0.0062	0.0020	360.0000	0.8960	417.7778
C28	0.0068	0.0021	372.0000	0.8990	427.7778
C29	0.0070	0.0021	382.0000	0.9020	436.1111
C30+	0.2234	0.0645	400.0000	0.9700	609.2340

## Appendix 2

Oil saturation along the slim-tube after 1PVI, for the near-miscible case, varying the number of components.




## References

- Arya, A., Hewett, T.A., Larson, R.G., Lake, L.W.: Dispersion and reservoir heterogeneity. *SPE Reserv. Eng.* **3**(01), 139–148 (1988)
- Chang, Y.-B., Lim, M., Pope, G., Sepehrnoori, K.: CO<sub>2</sub> flow patterns under multiphase flow: heterogeneous field-scale conditions. *SPE Reserv. Eng.* **9**(03), 208–216 (1994)
- CMG (2017) CMG-GEM technical manual. Computer Modelling Group
- Dykstra, H., Parsons, R.: The prediction of oil recovery by waterflood. *Second. Recovery Oil U. S.* **2**, 160–174 (1950)
- Gardner, J., Ypma, J.: An investigation of phase behavior-macroscopic bypassing interaction in CO<sub>2</sub> flooding. *Soc. Pet. Eng. J.* **24**(05), 508–520 (1984)
- Holm, L., Josendal, V.: Mechanisms of oil displacement by carbon dioxide. *J. Pet. Technol.* **26**(12), 1427–1438 (1974)
- Holm, L.W., Josendal, V.A.: Effect of oil composition on miscible-type displacement by carbon dioxide. *Soc. Pet. Eng. J.* **22**(01), 87–98 (1982)
- Jessen, K., Stenby, E.H., Orr Jr., F.M.: Interplay of phase behavior and numerical dispersion in finite-difference compositional simulation. *Soc. Pet. Eng. J.* **9**(2), 193–201 (2004)
- Khabibullin, R., Grin, Z.A., Alkan, H., Grivet, M., Elgridi, K.: Investigation of CO<sub>2</sub> application for enhanced oil recovery in a North African field—a new approach to EOS development. In: IOR 2017–19th European Symposium on Improved Oil Recovery (2017)
- Moortgat, J.: Viscous and gravitational fingering in multiphase compositional and compressible flow. *Adv. Water Resour.* **89**(Supplement C), 53–66 (2016)
- Orr, F.M.: *Theory of Gas Injection Processes*. Tie-Line Publications, Holte (2007)
- Sorbie, K.S., Mackay, E.J.: Mixing of injected, connate and aquifer brines in waterflooding and its relevance to oilfield scaling. *J. Pet. Sci. Eng.* **27**(1), 85–106 (2000)
- Stalkup, F.: Predicting the effect of continued gas enrichment above the MME on oil recovery in enriched hydrocarbon gas floods. In: *SPE Annual Technical Conference and Exhibition* (1998)
- Stalkup, F.I.: *Miscible Displacement*. SPE Monograph, Henry L. Doherty Series, vol. 8. Richardson, Texas (1983)
- Stalkup, F.L.: Effect of gas enrichment and numerical dispersion on enriched-gas-drive predictions. *SPE Reserv. Eng.* **5**(04), 647–655 (1990)
- Waggoner, J., Castillo, J., Lake, L.W.: Simulation of EOR processes in stochastically generated permeable media. *SPE Form. Eval.* **7**(02), 173–180 (1992)
- Wang, G., Pickup, G.E., Sorbie, K.S., Mackay, E.J.: “The analysis of compositional effects on global flow regimes in CO<sub>2</sub> near-miscible displacements in heterogeneous systems” dataset for paper SPE-190273 (2018). <https://doi.org/10.17861/fc1c90bb-9d3f-4a6c-9170-7b7fe10ec7b9>. <https://researchportal.hw.ac.uk/en/datasets/the-analysis-of-compositional-effects-on-global-flow-regimes-in-c>. Accessed 18 Jan 2019
- Wang, G., Pickup, G.E., Sorbie, K.S., Mackay, E.J.: Detailed assessment of compositional and interfacial tension effects on the fluid behaviour during immiscible and near-miscible CO<sub>2</sub> continuous and WAG displacements. *Transp. Porous Media* (2019a) (**accepted for publication**)
- Wang, G., Pickup, G.E., Sorbie, K.S., Mackay, E.J., Skauge, A.: Analysis of near-miscible CO<sub>2</sub>-WAG displacements: the distinction between compositional and interfacial tension effects SPE-193907. In: *SPE Reservoir Simulation Conference*. Society of Petroleum Engineering (2019b)
- Yellig, W., Metcalfe, R.: Determination and prediction of CO<sub>2</sub> minimum miscibility pressures (includes associated paper 8876). *J. Pet. Technol.* **32**(01), 160–168 (1980)

**Publisher's Note** Springer Nature remains neutral with regard to jurisdictional claims in published maps and institutional affiliations.

## Affiliations

G. Wang<sup>1</sup>  · G. E. Pickup<sup>1</sup> · K. S. Sorbie<sup>1</sup> · E. J. Mackay<sup>1</sup>

✉ G. Wang  
gw72@hw.ac.uk

<sup>1</sup> Heriot-Watt University, Riccarton, Edinburgh EH14 4AS, Scotland, UK